Journal Name

ARTICLE TYPE

Cite this: DOI: 00.0000/xxxxxxxxxx

Modelling and Fabrication of Wide Temperature Range $Al_{0.24}Ga_{0.76}As/GaAs$ Hall Magnetic Sensors

Hua Fan,[a,f,*] Huichao Yue,[a] Jiangmin Mao,[a] Ting Peng,[b,*] Siming Zuo,[c] Quanyuan Feng,[d] Qi Wei,[e,*] Hadi Heidari.[c]

Received Date
Accepted Date

DOI: 00.0000/xxxxxxxxxx

Silicon Hall-effect sensors have been widely used in industry and research fields due to their straightforward fabrication process and CMOS compatibility. However, as their material property limitations, technicians usually implement complex CMOS circuits to improve the sensors' performance including temperature drift and offset compensation for fitting tough situation, but it is no doubt that it increases the design complexity and the sensor area. Gallium arsenide (*GaAs*) is a superior material of Hall-effect device because of its large mobility and stable temperature characteristics. Concerning there is no specified modelling of *GaAs* Hall-effect device, this paper investigated its modelling by using finite element method (*FEM*) software Silvaco TCAD® to help and guide *GaAs* Hall-effect device fabrication. The modeled sensor has been fabricated and its experimental results are in agreement with the simulation results. Comparing to our previous silicon Hall-effect sensor, the *GaAs* Hall-effect sensor demonstrates potential and reliable benchmark for the future Hall magnetic sensor developments.

1 Introduction

Hall effect sensors have dominated most markets of magnetic sensors over the past several decades because of their high performance, small physical size and low cost. Their various applications such as an electronic compass, position detecting, current sensing, and contactless switching have made them the most popular type of magnetic devices. This is even truer since silicon Hall sensors are easily integrated on complementary metal oxide technology (CMOS) wafers with the readout electronics[1-4]. Generally, the Hall sensors enjoy wide detection range from 10 u *T* to 20 *T*, high spatial resolution smaller than 1 u*m*, and a wide band-width from DC to over 1 *MHz*[5]. However, with the increased use of Hall effect sensors both in industry and research fields, studying higher performance materials and fabrication process for Hall effect sensors becomes super important.

We have previously demonstrated a high-performance Hall sensor in CMOS technology with its integrated readout circuit [2].

According to our experience on CMOS hall sensors, the mobility is a critical material parameter of Hall-effect device, because large mobility Hall-effect device always means large sensitivity and low power consumption. Table 1 shows the electron mobility and energy gap of four common materials of Hall-effect devices and Gallium nitride (*GaN*) studied recently for Hall-effect devices[6,7]. In mobility, *Si* < *GaN* < *GaAs* < *InAs* < *InSb*[8]. According to the positive correlation between the drift velocity of carriers and the electron mobility, higher carrier mobility can bring higher magnetic sensitivity of the Hall device. Although Indium arsenide (*InAs*) and Indium Antimonide (*InSb*) have ultra-high mobility, their narrow energy gap leads to bad temperature performance and limits their applications. *GaAs* is a superior material for Hall-effect device, as it has large mobility and energy gap. *GaAs* Hall-effect sensors have emerged in previous decades, but they are not popular as silicon Hall-effect sensor because of their high price. However, the technology has been attracted a lot of attention in recent years, because it is an outstanding material for radio frequency (RF) and microwave components, and 5G communication technology promotes its development. The studying of high performances *GaAs* Hall-effect sensors are becoming gradually burning issues at present. A *GaAs* Hall-effect sensor with a compact design — an amplifier consisting of 5 pseudomorphic High Electron Mobility Transistors (pHEMT) and bias circuits consisting of a pHEMT and 2 diodes — can obtain the performance better than mature commercial low-noise CMOS Hall-effect sensor, and it can detect the magnetic field as low as 177 nT[9].After combining the noise suppression circuits, *GaAs* Hall-effect sensor is able to detect the magnetic field as low as 30 *nT*[10].

* Corresponding authors: fanhua7531@163.com, weiqi@tsinghua.edu.cn, pengt@hiwafer.com

a. State Key Laboratory of Electronic Thin Films and Integrated Devices, University of Electronic Science and Technology of China, Chengdu, China. e-mail: fanhua7531@163.com; yuehc99@163.com; jiangmin_mao@163.com

[b] Chengdu HiWafer Semiconductor Co., Ltd, e-mail:pengt@hiwafer.com

[c] James Watt School of Engineering, University of Glasgow, G12 8QQ, Glasgow, UK. e-mail: z.siming.1@research.gla.ac.uk; hadi.heidari@glasgow.ac.uk

[d] Southwest Jiaotong University, chengdu, china. e-mail:fengquanyuan@163.com

[e] Department of Precision Instrument, Tsinghua University, Beijing, China. e-mail:weiqi@tsinghua.edu.cn

[f] Institute of Electronic and Information Engineering of UESTC in Guangdong, University of Electronic Science and Technology of China, Dongguan, China

Table 1 Comparison of five materials of Hall-effect devices.

Material	*Electron mobility* ($cm^2/V/)s$	*Energy gap (eV)*
Silicon	1350	1.1
GaN	1600	3.39
GaAs	8500	1.43
InAs	40000	0.36
InSb	78000	0.17

In addition, other benefits of *GaAs* based Hall sensors include: (a) a high Hall constant about 6250 $cm^{-3}C^{-1}$with an electron concentration of 10^{15} cm^{-3}; (b)a high thermal conductivity about 0.81 Wcm^{-1} K^{-1}, utilizing an advantage of the heat released in the epitaxial layer; (c) almost any custom shape can be achieved in photolithographic nanofabrication process; (e) an excellent temperature stability due to the 1.4 eV energy gap of *GaAs* at 300 K; (d) a high resistivity about 10^5 $\Omega \cdot cm$; and (e) an ultra-thin thickness without changing desired properties of the bulk materials.

Considering there is no specified modelling of *GaAs* Hall-effect device, in this paper, a constant voltage bias modelling of *GaAs* Hall-effect device is presented by using commercial finite element method (*FEM*) software Silvaco TCAD® to guide and further study the *GaAs* Hall effect sensor. The device has been fabricated, and its experimental results of sensitivity performance and temperature performance are compared with simulation results. The important thing is that this model can also be used for the simulation of Hall sensors made of materials such as *Si, Ga* and *InSb*. In the design process, we can choose different types of materials, and we can also choose the corresponding electron mobility according to different manufacturing processes.

The layer structure of our Hall magnetic sensor is shown in figure 1. The 300 *nm* N+ *GaAs* with 10^{17} cm^{-3} uniform Si doping is the active layer to induce Hall output, and it is also used to form ohmic-contact with metal wire. *AlGaAs* has a larger band gap than *GaAs*, which can form a barrier to prevent the migration of electrons. The 20 *nm* $Al_{0.24}Ga_{0.76}As$ is used as the barrier layer to make electron be restricted in N+ *GaAs* space. Periodic $Al_{0.24}Ga_{0.76}As$ and *GaAs* form a superlattice structure which is used as a buffer layer and to produce periodic barriers for further preventing current flowing away from the substrate. The bottom layer is the *GaAs* substrate which is to provide mechanical strength and grow high quality *GaAs* epilayer.

2 Hall Effect Modelling

The Hall-effect sensor is based on the physical effect produced by a current-carrying semiconductor in a magnetic field. Its output voltage is directly proportional to the magnetic field strength. Currently, the cross-shaped model is widely employed as an optimum geometry to achieve the highest sensitivity and lowest offset[2]. In addition, such symmetric geometry can dramatically decrease the mismatch resulting from the fabrication process[11]. In our model, a conventional constant voltage bias Hall sensor is adopted, which can reduce the design complexity of bias circuit[7]. A

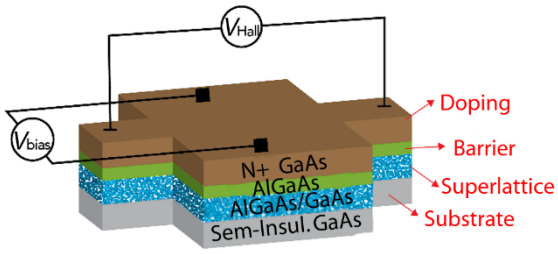

Fig. 1 *GaAs* Hall-effect sensor layers structures.

constant voltage supply (V_{bias}) is utilized to bias the Hall-effect sensor and then an output voltage (V_{hall}) as a result of an external magnetic field is measured at terminals. The Hall voltage with a voltage biasing can be expressed as[11]

$$V_{\text{Hall}} \cong \mu_H G_H \frac{W}{L} B V_{bias} \tag{1}$$

Where μ_H denotes the Hall mobility of majority carriers, W and L represent the width and length of the sensor respectively, B is the external magnetic field vertical to the device surface, G_H is the geometrical correction factor of Hall voltages. G_H is usually determined by the actual sensor structure and the shape of the contact pole, and the value range is $0 < G_H < 1$. For a sensor structure that is shaped like a crisscross type and whose rotating 90° structure remains unchanged, the structure factor can be approximated by the following equation 2:

$$G_H = 1 - 1.045\exp(-\frac{\pi(L-W)}{2W})\frac{\theta_H}{\tan\theta_H} \tag{2}$$

where θ_H denotes the Hall angle. Reducing the width-to-length ratio W/L of the Hall device can improve the device geometrical correction factor, which will also improve the sensor performance. However, as the width of the Hall device increases, the area of the sensor increases accordingly. Therefore, it is necessary to compromise the aspect ratio of the device within an appropriate range. For a cross-type horizontal Hall sensor, G_H value can usually reach approximately 1. In addition, the absolute sensor sensitivity can be defined from the equation 3. The sensitivity depending on the voltage output quantity can be given by[12]:

$$S_{Av} = \frac{V_{Hall}}{B} \qquad [\frac{V}{T}] \tag{3}$$

which represents the capability of the sensor to convert the magnetic field into a Hall voltage. For eliminating the influence of bias voltage on device sensitivity, the relative sensitivity is finally defined as the equation 4 dividing by the bias voltage, shown below[12]:

$$S_{Vv} = \left|\frac{V_{Hall}}{V_{bias} \times B}\right| \qquad [\frac{V}{VT}] = T^{-1} \tag{4}$$

In FEM, the quantity relationship of Hall-effect is defined in equation 5[13]:

$$\begin{bmatrix} J_x \\ J_y \\ J_z \end{bmatrix} = \frac{1}{1+\mu_H^2 B_z^2} \begin{bmatrix} 1 & -\mu_H B_z & 0 \\ \mu_H B_z & 1 & 0 \\ 0 & 0 & 1+\mu_H^2 B_z^2 \end{bmatrix} \begin{bmatrix} J_{x0} \\ J_{y0} \\ J_{z0} \end{bmatrix} \tag{5}$$

When an external magnetic field applied, the changes of current density $[J_x \ \ J_y \ \ J_z]^T$ are equal to multiplying a tensor, where $[J_{x0} \ \ J_{y0} \ \ J_{z0}]^T$ are the instinct current with no magnetic field. The tensor is consisted with magnetic field B_z and Hall mobility μ_H which is equal to the Hall scattering factor multiply carrier mobility. The classical value of Hall scattering factor is about 1.1 in this situation[13]. 8500 $cm^2/V/s$ electronic mobility of $GaAs$ can be adopted in the modelling. However, concerning mobility is a doping and temperature dependent parameter, its specified physical model should be consider-ed for accuracy modelling. In order to simplify the calculation, the mobility approximation is used to replace the Hall mobility in most cases. Both Hall mobility and mobility are related to temperature and doping. The Caughey-Thomas model is shown in equations 6 represents the change of Hall mobility with temperature and doping.

$$\mu_n = \mu_{\min} \cdot \left(\frac{TL}{300}\right)^{\alpha} + \frac{\mu_{\max} \cdot \left(\frac{TL}{300}\right)^{-\beta} - \mu_{\max}\left(\frac{TL}{300}\right)^{\alpha}}{1+\mu_{\max}\left(\frac{TL}{300}\right)^{\gamma} \cdot \left(\frac{N}{N0}\right)^{-\delta}} \tag{6}$$

where μ_{min} and μ_{max} represent the mobility saturation at the highest and lowest doping concentrate respectively, N_0 denotes the doping concentrate at which mobility reduces to half of μ_{max} value, N denotes the concentration of ionized donors. TL denote the lattice temperature. $\alpha, \beta, \gamma, \delta$ are adjustment parameters[14]. In Caughey-Thomas mobility model of Silvaco, μ_{min} = 500, μ_{max} = 8600, α = 0, β =−2.1, γ =−1.182, δ = 0.394, $N_0 = 6 \times 10^{16} cm^{-3}$. In[14], μ_{min} = 500, μ_{max} = 9400, α = 0, β = -2.1, γ = -1.182, δ = 0.394, $N_0 = 6 \times 10^{16} cm^{-3}$, μ_{max} = 9400, meaning they use the Hall mobility and assume $\mu \sim \mu_H$.

3 Simulation and Experimental Results

COMSOL Multiphysics is a multiphysics simulation software based on finite element analysis methods, which can simulate and analyze actual engineering problems involved in many fields including electromagnetics, structural mechanics, acoustics, fluid mechanics, and thermals. Because the COMSOL finite element simulation software has a parameter scanning function, COMSOL is used to explore the geometric factors of the Hall element. The shape of the fully symmetrical cross Hall element is shown in figure 2(a). The input and output ports have the same length L and width W. When studying this structure, the ratio of W and h is more commonly used instead of length L and width W as the abscissa of the coordinate axis. The simulation result is shown in figure 2(b). At the beginning, the Hall voltage increases with W/h. When W/h is about 3, the sensitivity of the fully symmetrical cross-shaped Hall disk is the greatest. When W/h is greater than 3, the Hall voltage tends to decrease. The narrow cross-shaped Hall element studied in this paper is shown in figure 3 (a), which is similar in shape to a fully symmetrical cross-shaped Hall plate, but the output interface is narrower. Because the width and length of the output port have a small effect on the input resistance, it has a small effect on the static operating point of the Hall element. Therefore, this paper studies the influence of the changes in the width W' and length L' of the output port of the narrow cross-shaped Hall element on the Hall voltage. Based on the fully symmetrical cross-shaped Hall plate when the W/h is about 3 and the Hall voltage output is the maximum. Take the fully symmetrical cross-shaped Hall element at the maximum W/h of 3 Hall voltage output as the reference. By changing the width of the output port of the reference Hall element, the Hall voltage of the narrow cross Hall element in figure 3(b) varies with the width of the output port. It can be concluded that the smaller the output port, the greater the Hall voltage. When W'/W = 0.5, that is, when the output port is half of the input port, the Hall voltage output growth tends to slow down as W'/W decreases.

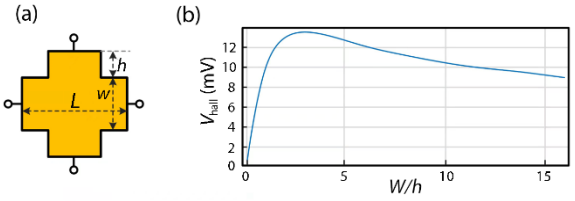

Fig. 2 (a) Fully symmetrical cross-shaped Hall element; (b)The Hall voltage of the fully symmetrical cross Hall element changes with the shape.

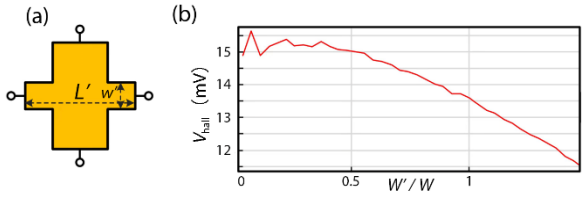

Fig. 3 (a) Narrow cross-shaped Hall element; (b) The Hall volt-age of the narrow cross Hall element varies with the width of the output port.

Numerical simulation of the Hall-effect sensor is performed using Silvaco TCAD®. Previous simulations of Hall sensors are summarized in[15]. Figure 4 shows our proposed structure of the Hall-effect sensor. The color legend indicates the surface potential distribution by applying a magnetic field of 100 mT. The model geometry of the Hall sensor has been simulated without any mismatch. The ground and supply voltage are added to cathode and anode of Hall-effect sensor.

The 2D and 1D electrons distribute of vertical cut-plane are demonstrated in figure 5 (a) and figure 5 (b). Although $Al_{0.24}Ga_{0.76}As$ is just below the N+ doping epilayer, it almost has no carrier because of its larger energy gap barrier which stops carriers in $GaAs$ flowing to $Al_xGa_{1-x}As$. So the electrons are inside the potential well. Electrons are restricted in the thin N+ $GaAs$

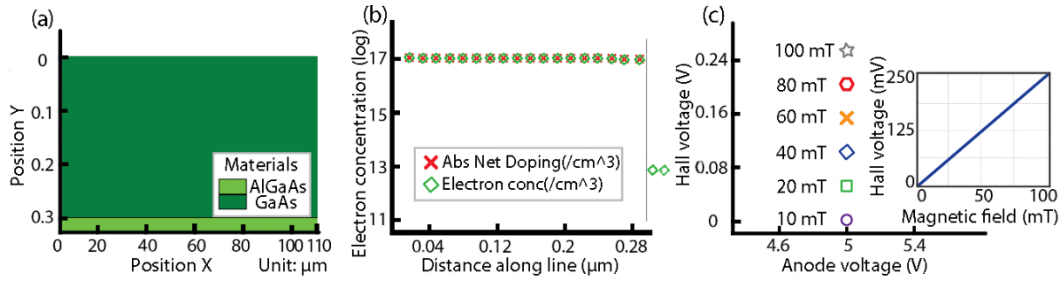

Fig. 5 (a) The 2D vertical cut-plane of Hall-effect sensor. *GaAs* layer (bottle green) is the doping layer and $Al_xGa_{1-x}As/GaAs$ (green) is the channel layer; (b) Electrons distribution of 2DEG *GaAs* Hall-effect sensor in 1D when a $5V$ supply voltage is added; (c) simulated output voltage of $Al_xGa_{1-x}As/GaAs$ Hall sensor.

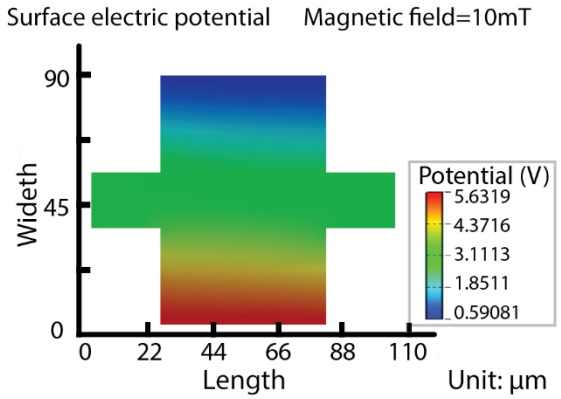

Fig. 4 GaAs Hall-effect sensor built in Silvaco TCAD.

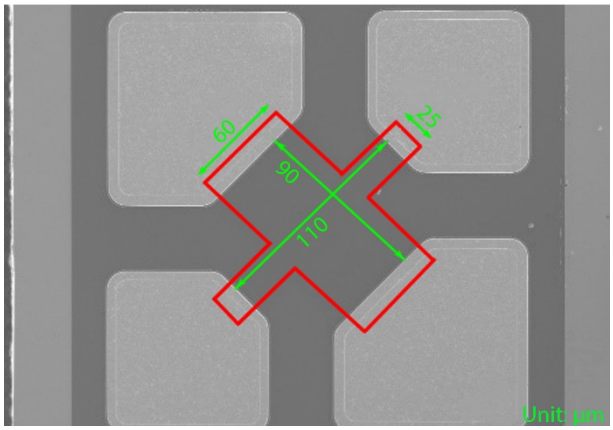

Fig. 6 Fabricated $Al_xGa_{1\_x}As/GaAs$ Hall sensor microphotograph.

channel, which forms the two-dimensional electron gas (2DEG) structure confined in the potential well near $Al_xGa_{1-x}As/GaAs$ interface. The final output voltage of the Hall sensor is demonstrated in figure 5 (c). The value of y-axis represents the Hall voltage. It is noted that the output is linearly increased by changing the magnetic field from the 0 to 100 mT . The voltage response is very linear, and the maximum output voltage of 0.25 V is obtained. The sensitivity of the Hall effect device is 0.51 $V/V/T$.

Figure 6 illustrates the microphotograph of the Hall-effect sensor. The red line cross-shape represents the active region of device, but the effective region of device doesn't include pads in white color, and its maximum width and length are 110 μm and 90 μm respectively. The sensor manufacture is compatible with pHEMT processing technology[9]. There are 4 main steps in its manufacture. Firstly, isolating the device through implant Boron. Secondly, $Au/Pt/Ti$ metals are grown on N+ *GaAs* epilayer, which is used to form Ohmic contact—a classic contact for avoiding forming nonlinear *I-V* relationship between the metal and the semiconductor. Thirdly, Si_3N_4 is deposited on the wafer surface and etched in the pad to protect the device. Finally, A metal wire is grown for its connection to circuits.

During the experiment, electromagnet Helmholtz coil is used inducing magnetic field. Hall effect sensor is put in the center of Helmholtz coil for obtaining a relatively constant magnetic field, and there has no consideration for shielding geomagnetic, because it induces the Hall voltage less than 0.1 mV . Guassmeter HT208 (0.1 μT resolution) from Hengtong Inc. is used to measure induced magnetic fields from the coils. In terms of temperature performance, temperature chamber CST842T from Hhtesting Inc. is used to generate temperature from −75 to 200 °C, providing a constant temperature environment. The measured sensitivity at room temperature is shown in figure 7 (a). The average is 0.28 $V/V/T$, which is in the same order of magnitude as the simulation result, but it still has large mismatch, so the model resolution should be improved, which will be further discussed.

Moreover, the temperature dependence of the final output voltages are shown in figure 7 (b), with the temperature ranging from −40 to 150 °C at 50mT vertical magnetic field. The highest measured value of the Hall voltage is V_H = 72.5 mV at −40 °C. In addition, it is clearly noticed that the output signal slightly drops as the temperature increases. It is worth mentioning that the increasing temperature brings about the raise of carrier scattering, which leads the decrease of carrier mobility of Hall sensor. Therefore, the higher the temperature, the smaller the

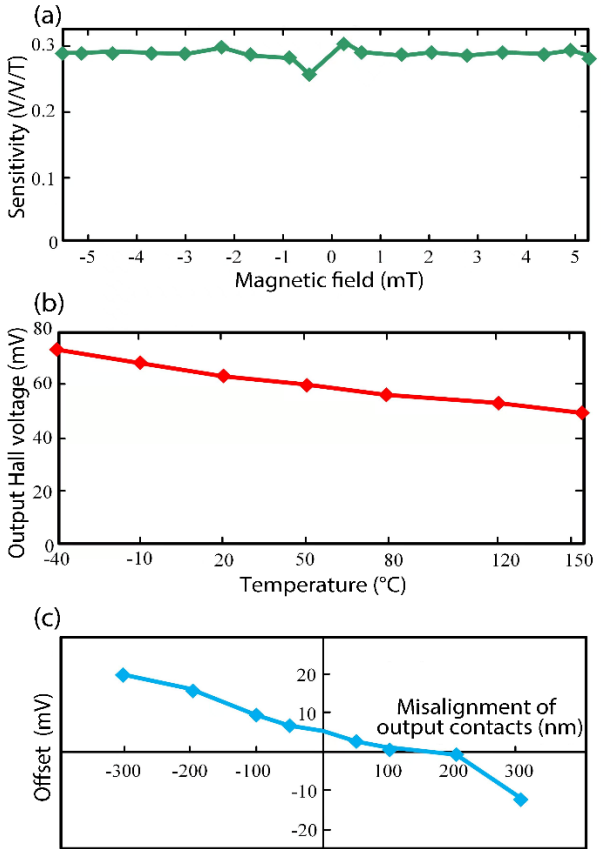

Fig. 7 (a) Simulated sensitivity of the voltage-mode Hall sensor; (b) Dependence of temperature on output voltage; (c) simulated offset with different misalignment of output contacts.

carrier mobility, which results in the lower Hall output voltage.

Finally, figure 7 (c) performs the offset with different misalignment of output contacts from −300 *nm* to 300 *nm* to find the lowest offset. The measurement is at room temperature and the external applied magnetic field is zero. Ideally, non-misalignment of output contacts will obtain zero output voltage. However, non-ideal factors of piezoelectric effect and discontinuity of material will result in an asymmetry of the device property and then generate offset voltage. It can be alleviated by misaligning output contacts. The offset is equal to 5 mV when the misalignment is zero. When there is 100 *nm* mismatch, the device approximately has the lowest offset zero. Subsequently, a standard CMOS-based analogue front-end circuit comprises of an operational amplifier and a low-pass filter could achieve on-chip noise and offset suppression.

If only using the Shockley-Read-Hall Recombination model, a common model in semiconductor, it can obtain 0.44 $V/V/T$ sensitivity, which leads to large error compared with 0.28 $V/V/T$ in experimental results. Aiming at narrowing the difference between the simulation and experimental results, models need to be improved. Considering the 5, carrier mobility u must be corrected. It is higher in previous simulation work. Carrier mobility is always related with the temperature and the doping concentrate, so analytic physical model is used to correct the device modelling. The quantity relationship of analytic physical model is defined in 6, where μ_1 , μ_2 ,α, β , γ, δ,N_0 are constant parameters related to material property and they can be obtained in the datasheet. TL and N are lattice temperature and carrier concentrate respectively, which are related to the user defined doping concentrate and temperature. On the other hand, the simulation model of Hall device is specified into 3 sub-models according to its epilayers. Single $GaAs$ layer simulation, $GaAs$ and $Al_xGa_{1-x}As$ two-layer simulation, and all epilayers simulation are built for studying the model pithily, effectively and accurately.

Table 2 The comparison of simulation results and experimental results at 300K

	Caughey-Thomas[16]	Caughey-Thomas[13]	Experiment
Mobility $(cm^2/V/s)$	4144	4504	4480
Hall Mobility $(cm^2/V/s)$	4558	4504	5010
Sensitivity $(V/V/T)$	0.26	0.24	0.28
Absolute sensitivity (V/T)	1.32	1.2	1.38

Figure 8(a ,b) shows the new simulation results of Hall outputs. In order to explore the difference between $GaAs$ Hall sensor and $Al_{0.24}Ga_{0.76}As/GaAs$ Hall Sensors, we further conducted some tests on individual $GaAs$ Hall devices to explore the influence of $Al_{0.24}Ga_{0.76}As$ layer on the sensor. The experimental results are also added for comparison. The two different epilayer simulations show slight differences. That means only $GaAs$ channel layer needs to be considered, which can effectively reduce the simulation complexity and time. It also shows $Al_xGa_{1-x}As$ is a suitable barrier material to form 2DEG. After considering analytic physical model, the simulation results are highly in consistent with the experimental results. The simulated sensitivity is also $0.28V/V/T$. Furthermore, simulation results are shown in figure 8 (b), which are in consistent with the experimental results after using analytic physical mode.

Table 2 summaries and compares simulation results using the Caughey-Thomas model with different parameters and our experimental results at 300 K. Regarding the mobility and Hall mobility,[16] and[13] are relatively low. We used the Caughey-Thomas mobility model provided in Reference 13 and got a voltage sensitivity of 0.24 $V/V/T$. We used another Caughey-Thomas mobility model provided by Dr Hadi Heidari in 16 and got a voltage sensitivity of 0.26 $V/V/T$. If only using the common model in semiconductor, it can obtain 0.44 $V/V/T$ sensitivity, but it leads to large error compared with 0.28 $V/V/T$ in experimental results. It can be seen that we have obtained more accurate sensitivity after we have corrected the mobility model.

Table 3 summaries specifications of our fabricated $Al_{0.24}Ga_{0.76}As/GaAs$ Hall-effect sensor and compares with other works in terms of the sensitivity, offset, and input/output resistances. From the experimental results of our developed Hall sensor, four times higher sensitivity has been achieved compared to the state-of-the-art Hall sensors based on silicon[15] and GaN[7]. It operates at the highest absolute sensitivity of 1.38 V/T. Also, it

Table 3 The comparison of different types of Hall-effect devices.

	Jovanovic[15]	Dowling[7]	Jankowski[17]	Haned[9]	Wouters[18]	**This work**
Material	Si	GaN	InSb	GaAs/InGaAs	GaAs	GaAs
Power Supply (V)	0.4-0.5	0.04-0.5	0.5mV	1.75	0.074	5
Sensitivity ($V/V/T$)	0.043	0.057	2 ($V/A/T$)	400 ($V/A/T$)	100-107 ($V/A/T$)	0.28
Absolute sensitivity (V/T)	0.0172-0.0215	0.00228-0.0285	0.1	0.4	<0.0107	1.38
Offset (mV)	19.47	20 (nV)	-	0.14	2-80	5
Input Resistance (kW)	-	1.56	0.01	1.75	0.65-0.74	1.2
Output Resistance (kW)	-	1.56	0.01	1.75	0.65-0.74	2.4

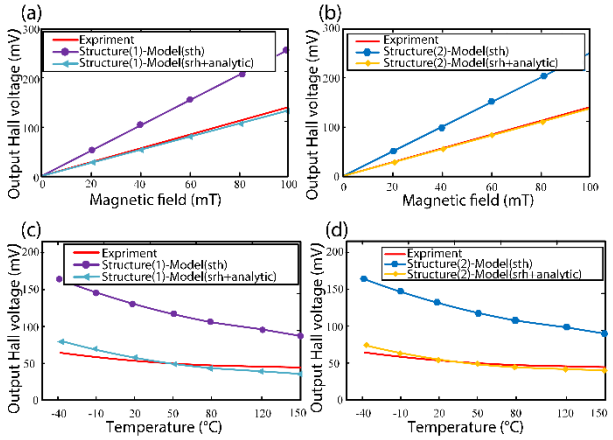

Fig. 8 Combining 2 types of epilayer structure and 2 physical models, 4 simulation results are presented. Experiment results are added for comparison with, **(a,b)** magnetic field and **(c,d)** temperature (50 mT).

it achieves a relatively low offset compared with the *GaAs* Hall-effect device in[18]. Table generated by Excel2LaTeX from sheet 'Sheet1'

The simulations results are highly consistent with the experimental output. $\mu_{min} = 500$, $\mu_{max} = 8600$, $\alpha = 0$, $\beta = -2.1$, $\gamma = -1.182$, $\delta = 0.394$, $N_0 = 6 \times 10^{16} cm^{-3}$ are adopted for fitting the experimental data.

4 Conclusions

We have developed a *GaAs* based Hall sensor and its constant voltage-bias modelling. We used the COMSOL multiphysics simulation tool to study the influence of geometry on the Hall voltage. It is found that the sensitivity of the fully symmetrical Hall element is optimal when W/h is equal to 3. Studies have found that the sensitivity of the narrow cross is better than that of a fully symmetrical Hall element, and it is optimal when the length of the long contact port is twice the length of the short contact port.The cross-shaped Hall sensor has been simulated using Silvaco TCAD® to investigate the sensitivity and temperature performance. Simulation results are highly in consistent with the experimental results. The high sensitivity of 0.28 $V/V/T$ is obtained from the experiment with a low offset of 5 mV . A high absolute sensitivity of 1.38 V/T is achieved at 5 V bias voltage. Moreover, the temperature dependence of the Hall sensor is investigated for the maximum Hall voltage of 72.5 mV and the sensitivity of 0.275 $V/V/T$ at −40 °C. The future work will focus on the design and implementation of a whole Hall microsystem with readout circuits using standard CMOS technology.

Acknowledgment

The work of Hua Fan was supported by the National Natural Science Foundation of China (NSFC) under Grant 61771111, supported by Sichuan Provincial Science and Technology Important Projects under Grant 22ZDYF2805, supported by the Open Foundation of the State Key Laboratory of Electronic Thin Films and Integrated Devices under Grant KFJJ202006, and supported by Intelligent Terminal Key Laboratory of Sichuan Province under Grant SCITLAB-1001.

The work of Quanyuan Feng was supported by Major Project of the National Natural Science Foundation of China under Grant 62090012.

Notes and references

1 R. Popovic, Z. Randjelovic and D. Manic, Integrated Hall-effect magnetic sensors, Sensors and Actuators A Physical, 2001, **91**, 46 – 50.

2 H. Heidari, E. Bonizzoni, U. Gatti and F. Maloberti, A CMOS Current-Mode Magnetic Hall Sensor With Integrated Front-End, Circuits and Systems I: Regular Papers, IEEE Transactions on, 2015, **62**, 1270–1278.

3 M. Pastre, M. Kayal and H. Blanchard, A Hall Sensor Analog Front End for Current Measurement With Continuous Gain Calibration, IEEE Sensors Journal,2007, **7**, 860–867.

4 A. Ajbl, M. Pastre and M. Kayal, A fully integrated Hall sensor microsystem for contactless current measurement, SENSORS, 2012 IEEE, 2012, pp. 1–4.

5 Z. B. Randjelovic, M. Kayal, R. Popovic and H. Blanchard, Highly sensitive Hall magnetic sensor microsystem in CMOS technology, IEEE Journal of Solid-State Circuits,2002, **37**, 151–159.

6 K. M. Dowling, H. S. Alpert, A. S. Yalamarthy, P. F. Satterthwaite, S. Kumar, H. Köck, U. Ausserlechner and D. G. Senesky, Micro-Tesla Offset in Thermally Stable AlGaN/GaN 2DEG Hall Plates Using Current Spinning, IEEE Sensors Letters, 2019, **3**, 1–4.

7 K. M. Dowling, H. A. Alpert, P. Zhang, A. Ramirez and D. G. Senesky, The effect of bias conditions ON AlGaN/GaN 2DEG hall plates, 2018 Solid-State, Actuators, and Microsystems Workshop, 2018.

8 S. Sze, SERBIULA (sistema Librum 2.0), Physics of Semiconductor Devices. New York , SERBIULA(sistema Librum 2.0) 1981, **1**,.

9 N. Haned and M. Missous, Nano-tesla magnetic field magnetometry using an InGaAs\-AlGaAs\-GaAs 2DEG Hall sensor, Sensors and Actuators A: Physical, 2003, **102**, 216 – 222.

10 V. Mosser, N. Matringe and Y. Haddab, A Spinning Current Circuit for Hall Measurements Down to the Nanotesla Range, IEEE Transactions on Instrumentation and Measurement, 2017, **66**, 637–650.

11 H. Heidari, E. Bonizzoni, U. Gatti, F. Maloberti and R. Dahiya, CMOS Vertical Hall Magnetic Sensors on Flexible Substrate, IEEE Sensors Journal, 2016, **16**, 8736–8743.

12 H. Heidari, E. Bonizzoni, U. Gatti and F. Maloberti, A 0.18-*μm* CMOS current-mode Hall magnetic sensor with very low bias current and high sensitive front-end , SENSORS, 2014 IEEE, 2014, pp. 1467–1470.

13 W. Allegretto, A. Nathan and H. Baltes, Numerical analysis of magnetic-field-sensitive bipolar devices, IEEE Transactions on Computer-Aided Design of Integrated Circuits and Systems, 1991, **10**, 501–5.

14 M. Sotoodeh, A. Khalid and A. Rezazadeh, Empirical low-field mobility model for III-V compounds applicable in device simulation codes , Journal of AppliedPhysics, 2000, **87**, 2890–2900.

15 E. Jovanovic, T. Pesic and D. Pantic, Dragan, 3D simulation of cross-shaped Hall sensor and its equivalent circuit model, Proceedings of the International Conference on Microelectronics 2004, pp. 235-238 vol.1.

16 H. Heidari, U. Gatti, E. Bonizzoni and F. Maloberti, Franco, Low-noise low-Offset current-mode Hall sensors, Conference Proceedings - 9th Conference on Ph. D. Research in Microelectronics and Electronics, PRIME 20132013, pp. 325–328.

17 J. Jankowski, S. El-Ahmar and M. Oszwa?dowski, Hall Sensors for Extreme Temperatures, Sensors (Basel, Switzerland), 2011, **11**, 876–85.

18 C. Wouters, V. Vrankovi, C. Rssler, S. Sidorov, K. Ensslin,W. Wegscheider and C. Hierold, Design and fabrication of an innovative three-axis Hall sensor, Sensors and Actuators A: Physical, 2016, **237**, 62–71.

Hua Fan (M'16) was born in Ziyang, Sichuan, China, in 1981. She received the B.S. degree in communications engineering and the M.S. degree in Computer science and technology, both from Southwest Jiaotong University, Chengdu, China, in 2003 and 2006, respectively. She received the Ph.D. degree from Tsinghua University, Beijing, in July 2013. From September 2013 to June 2016, she was an assistant professor of University of Electronic Science and Technology of China, from July 2016 to 2021, she was an associate professor of University of Electronic Science and Technology of China, Chengdu, China. From July 2021 to present, she is a professor of University of Electronic Science and Technology of China, Chengdu, China.

Huichao Yue was born in Gaocheng, Hebei, China, in 1999. He received the B.S. degree in Microelectronics science and technology from University of Electronic Science and Technology of China, Chengdu, China in 2021. From August 2021 to present, he is a master student of University of Electronic Science and Technology of China, Chengdu, China. His main research interest is Hall sensor.

Jiangmin Mao was born in Huaihua, Hunan, China, in 1995. He received the B.S. degree in microelectronic science and technology from Harbin Engineering University, Harbin, China, in 2017. From August 2017, he is making efforts for the master degree in integrated engineering in the School of Electronic Science and Technology at the University of Electronic Science and Technology of China, Chengdu, China. His research interests include Hall-effect sensor, magnetic device, sensor interface design, and digital system design.

Ting Peng received the B.S. degree in Physics and PH.D. degrees in Microelectronics and Solid State Electronics, from Wuhan University, Hubei, China, in 2005 and 2010, respectively. Since 2011, he has been working on the research and development of GaAs based electron devices and process, with GaAs Technology Department, Chengdu HiWafer Semiconductor Co. Ltd., where he is currently the Manager of the Department.

Siming Zuo is a Research Technician at the James Watt School of Engineering, University of Glasgow. He has submitted his PhD dissertation in January 2021 and will take up a Research Assistant post in meLAB from June 2021. His PhD on magnetomyography with spintronics led to multiple peer-review papers. He received the SFB 1261 Fellowship, Germany (2018). His work was recognized by a Best Paper Award from IEEE PrimeAsia'18 and two IEEE Travel Grants to attend ISCAS 2019 and 2020.

Quanyuan Feng(M'06–SM'08) received the M.S. degree in microelectronics and solid electronics from the University of Electronic Science and Technology of China, Chengdu, China, in 1991, and the Ph.D. degree in electromagnetic field and microwave technology from Southwest Jiaotong University, Chengdu, in 2000. He is currently the Head of the Institute of Micro-electronics, Southwest Jiaotong University.

Qi Wei received the Ph.D. degree from Tsinghua University, Beijing, China, in 2010 . He is currently an Assistant Professor with the Department of Electronic Engineering, Tsinghua University. His research interests include ME-MS inertial sensors, application-specific integrated circuit(ASIC) design, and high-performance data converters.

Hadi Heidari (S'11–M'15–SM'17) is an Assistant Professor (Lecturer) in the James Watt School of Engineering at the University of Glasgow, United Kingdom. His Microelectronics Lab (meLAB) consists of 3 postdoctoral researchers and 8 PhD students, conducts pioneering research on magneto electronics and integrated microelectronics design for wearable and implantable devices. He has authored over 150 articles in peer reviewed journals (e.g. IEEE Solid-State Circuits Journal, Trans. Circuits and Systems I and IEEE Trans. Electron Devices) and in international conferences.